Title

Synthetic Catalysts for Selective Glycan Cleavage from Glycoproteins and Cells.

Permalink

Journal

Authors

Zangiabadi, Milad

Bahrami, Foroogh

Ghosh, Avijit

et al.

Publication Date

DOI

Synthetic Catalysts for Selective Glycan Cleavage from Glycoproteins and Cells

Milad Zangiabadi[a], **Foroogh Bahrami**[a], **Avijit Ghosh**[a], **Hai Yu**[b], **Anand Kumar Agrahari**[b], **Xi Chen**[b], **Yan Zhao**[a]

[a]Department of Chemistry, Iowa State University, Ames, Iowa 50011, U.S.A.

[b]Department of Chemistry, University of California-Davis, One Shields Avenue, Davis, CA 95616, U.S.A.

Abstract

In situ modification of glycans requires extraordinary molecular recognition of highly complex and subtly different carbohydrates, followed by reactions at precise locations on the substrate. We here report synthetic catalysts that under physiological conditions cleave a predetermined oligosaccharide block such as a branched trimannose or the entire N-glycan of a glycoprotein, while nontargeted glycoproteins stay intact. The method also allows α2–6-sialylated galactosides to be removed preferentially over the α2–3 linked ones from cell surfaces, highlighting the potential of these synthetic glycosidases for glycan editing.

Graphical Abstract
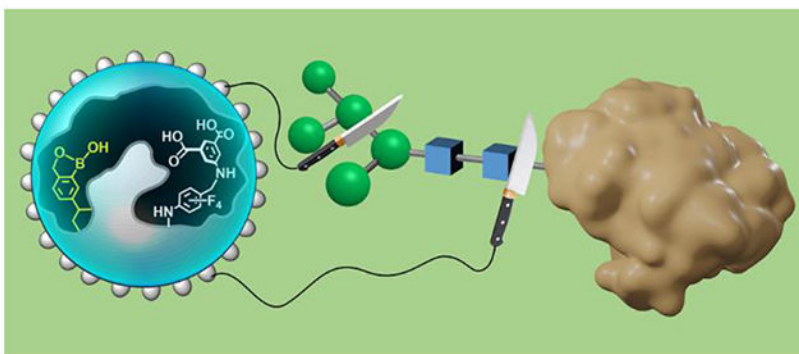
In situ modification of glycans or glyco-editing of glycoproteins, membrane, and cell surface is a powerful tool to elucidate the roles of specific glycans and alter the biological functions associated with them.[1–4] Glyco-editing requires molecular recognition of highly complex glycans from their subtly different structural analogues, followed by reactions at precise locations for the desired transformation. Since few chemical reagents have the

required selectivities,[5] enzymes such as glycosyltransferases,[6–10] exoglycosidases[2,11] and endoglycosidases[12] are the most popular tools. If nontargeted glycans made of similar building blocks and/or linkages are present along with the targeted ones, even enzymes become inadequate in their selectivities.

Glycan-recognizing materials can be prepared via molecular imprinting using boronic acid functional monomers (FMs).[13–17] Techniques are also available to control the orientation of the binding sites.[18–20] We herein report "artificial glycosidases",[21–28] specifically designed for highly selective glycan deletion. The method involves molecular imprinting of neoglycoconjugates such as **1a–b** in the mixed micelles of cross-linkable surfactants **5a/5b** using boroxole **2** as the FM (Scheme 1).[29,30] Photoaffinity labeling of the imprinted site using **4** via nitrene C–H insertion[31] installs an isophthalic acid moiety in the active site, mimicking the dicarboxylic acid motif of glycosidase.[32,33] MINPs are generally decorated with surface ligand **6a** for facile purification of the material (see SI for details).

Table 1 shows that as prepared $MINP_{Glc1}$ binds photoaffinity label **4** strongly (entry 1). ($MINP_{Glc1}$ and $MINP_{Glc2}$ refer to the MINP prepared with **1a** and **1b** as the template, respectively.) Successful imprinting is also supported by the 3.5 times stronger binding for glucose over maltose (entries 2–3) and the negligible binding of glucose by the nonimprinted nanoparticles (NINPs) (entry 15). After the photoaffinity labeling, the resulting $MINP_{Glc1}$-COOH binds the sugars more strongly (entries 4–5), likely due to additional hydrogen bonds formed between the guest and the nearby isophthalic acid of the covalently attached photoaffinity label. $MINP_{Glc2}$ shows a reversed selectivity, with a 7.6:1 ratio favoring maltose Glc_2, further supporting the success of the molecular imprinting (entries 7–8). Photo-functionalization of $MINP_{Glc2}$ (to form $MINP_{Glc2}$–COOH) again enhances the binding for both sugars while maintaining the selectivity towards Glc_2 (entries 9–10).

Amphiphilicity of the template suggests the imprinted site at the end will be close to the micelle surface. This is ideal for a glycan-cleaving catalyst, because it should be able to "bite" a predetermined block of sugars inside the imprinted active site and cleave it at the point of connection from the rest of the structure using its diacid group. Meanwhile, the rest of the larger sugar guest (the magenta-colored R in Scheme 1) should stay in the aqueous solution for proper solvation. (For the same reason, although the template molecule is mostly in the β form, the resulting MINP catalyst should cleave both α- and β-linked glycans.)

$MINP_{Glc1}$-COOH indeed cleaves maltose with ~80% yields over pH 4.5–6.5 but the yield drops precipitously over pH 6.5–7.0 (Figure S21a). Natural glycosidase employs a protonated carboxylic acid as a general acid and another deprotonated carboxylate as either a general base or a nucleophile to catalyze the cleavage of glycosidic bonds.[32,33] Optimal catalysis generally occurs between pH 4 and 6, and higher pHs cause deprotonation of the general acid and a loss of activity.[34,35] Our catalysts likely operate by a similar mechanism.

When used to break down maltotetraose, $MINP_{Glc1}$-COOH affords predominantly glucose (72%) as it removes one sugar residue at a time. Meanwhile, $MINP_{Glc1}$ without the photoaffinity label, $MINP_{Glc1}$ with the noncovalently bound photoaffinity label, the

photoaffinity label **4** by itself, or **4** in combination with NINPs display no activity (Figure 21b). $MINP_{Glc2}$-COOH, the catalyst designed to "bite off" Glc_2 units, yields maltose as the major product as expected (75%), with glucose as the minor product (7%). Both MINPs display Michaelis–Menten kinetics (Table S1, Figure S47). Consistent with the binding of the 4,6-diol by the boroxole group on the nonreducing end of glucose on the substrate, the catalytic efficiency of $MINP_{Glc1}$-COOH for maltose or maltulose is nearly 5 times higher than that for galactose-terminated lactose.

Editing of biological glycans is more demanding on the selectivity. Branched Man_3, for example, is not only found at the end of $Man_5GlcNAc_2$ (the most abundant glycan on avian ovalbumin or OVA),[36] but also at an internal branching point (Figure 1). Yet, $MINP_{Man3}$-COOH, prepared following similar procedures in Scheme 1 using Man_3 as the templating glycan, cleaves the terminal Man_3 selectively. The center of the peaks for OVA decreases by ~500 *m/z* units in the MALDI mass spectrum (Figure S30a,b), while the cleaved product shows a dominant peak for Man_3 (Figure S31). OVA has a single glycan on Asn-292.[36] The entire N-glycan can be cleaved by sodium hypochlorite, which destroys the protein structure at the same time.[37] Using the cleaved glycan mixture as the templates, we prepared $MINP_{OVA}$-COOH, which in principle should remove the entire N-glycan. To our delight, after MINP hydrolysis, the center of the OVA peaks decreases by about 1200 *m/z* units (Figure S30c), with $Man_5GlcNAc_2$ as the main cleaved product (Figure S32).

The glycans on OVA[36] and RNase B[38] are similar (i.e., high mannose type) but differ from those on transferrin (Tf)[39] and IgG.[40] When a mixture of OVA/BSA/Tf/IgG is treated with $MINP_{Man3}$-COOH and $MINP_{OVA}$-COOH, respectively, only OVA undergoes the desired editing (Figure 2a). When OVA and RNase B are present in the mixture of RNase B/OVA/BSA/Tf, both undergo the desired cleavages (Figure 2b). Horseradish peroxidase (HRP) has a similar M.W. as OVA. With its N-glycans mostly in the form of $(Xyl)_xMan_m(Fuc)_fGlcNAc_2$,[41] it is not cleaved under the same experimental conditions (Figure S33).

Sialic acids (Sia) are frequently found as terminal monosaccharides of biological glycans on the outer surface of cells.[42] Two wild-type sialidases are available based on their substrate selectivities—one selective toward α2–3-linked sialic acids and the other with broad specificity. There is a strong need to differentiate glycans terminated with α2–6-versus α2–3-sialyl linkages,[43,44] because these glycans are used by influenza viruses for infection and switching in the binding specificity for the two glycans is key to the crossover of the viruses from animals to human.[45]

Our method readily produces a synthetic endoglycosidase to cleave α2–6-linked sialic acids, using template **8a** made from disaccharide **7a** (Figure 1). The resulting $MINP_{7a}$-COOH cleaves Neu5Acα2–6Gal from trisaccharide **9** and more complex sialyglycopeptide (SGP) in ~70% yields while the nontargeted trisaccharide **10** stays completely intact. In contrast, $MINP_{7b}$-COOH prepared using the α2–3-linked **7b** as the templating sugar only cleaves the corresponding **10** without touching the mismatched **9** (Figures S34–46).

$MINP_{7a}$-COOH could also cleave α2–6-sialylated galactosides from cells. Figure 3a shows that MDA-MB-231 cells have both Neu5Acα2–6Gal (stained green) and Neu5Acα2–3Gal (stained red). Overlay of the green and red images indicates that many regions of the membranes have sialic acids with both sialyl linkages (showing a yellow/orange color) while isolated spots are enriched with one or the other. Consistent with the selectivities of the natural sialidases, the cells treated with α2–3-sialidase have the α2–3-linked sialic acids preferentially removed and the cells treated with the nonspecific sialidase both α2–3- and α2–6-linked sialic acids removed (Figure 3a, the middle two rows of images). Most importantly, the cells treated with $MINP_{7a}$-COOH has its green fluorescence significantly reduced over the red. As a result of the selective cleavage of Neu5Acα2–6Gal, the overlaid image is dominated with a red color (Figure 3a, last row of images), instead of yellow/orange in the untreated sample or green in the α2–3-sialidase-treated one.

The above selectivity was quantified by fluorescence-activated cell sorting (FACS). As shown in Figure 3b, $MINP_{7a}$-COOH lowers the green fluorescence of the stained cells (from Neu5Acα2–6Gal) by ~64%, similarly as the nonspecific sialidase (by 75%). Figure 3c shows that $MINP_{7a}$-COOH is practically unreactive toward Neu5Acα2–3Gal, since the red emission stays nearly unchanged from that of the untreated sample. (According to Figure 3a, α2–3-sialidase cleaves Neu5Acα2–3Gal efficiently from the cells. However, the spectral overlap between the green and red emissions and the 20 times stronger green emission interfere with detection in the red channel, which shows ca. 20% reduction in intensity for the α2–3-sialidase-treated sample in Figure 3c.)

It is economical for a cell to use a small number of exoglycosidases to break down diverse glycans to recycle the monosaccharides. When used for glycan editing, however, common glycosidases are severely limited due to their inability to differentiate glycans made of similar building blocks/linkages. Glycosidases are some of the most proficient enzymes in nature. The digestive maltase-glucoamylase, for example, has a catalytic efficiency of >7000 M^{-1} s^{-1},[46] whereas our comparable MINPs (for maltose or maltotetraose) have a value of 33–63 M^{-1} min^{-1} (Table S1). Although there is much room for improvement in activity, our catalysts do cleave natural glycans under physiological conditions with exquisite selectivity. Their custom-designed substrate-selectivity enables them to delete a predetermined block of sugars directly from glycoproteins or even cell surfaces. Facile one-step synthesis of the templates from unprotected glycans, the 2-day/1-pot preparation of MINP, and the straightforward photoaffinity labeling make them potentially very useful tools in glyco-editing.

Supplementary Material

Refer to Web version on PubMed Central for supplementary material.

ACKNOWLEDGMENT

REFERENCES

(1). Mahal LK; Yarema KJ; Bertozzi CR Engineering chemical reactivity on cell surfaces through oligosaccharide biosynthesis. Science 1997, 276, 1125–1128. [PubMed: 9173543]

(2). Xiao H; Woods EC; Vukojicic P; Bertozzi CR Precision glycocalyx editing as a strategy for cancer immunotherapy. Proc. Natl. Acad. Sci. U. S. A 2016, 113, 10304–10309. [PubMed: 27551071]

(3). Zeng Y; Tang F; Shi W; Dong Q; Huang W Recent advances in synthetic glycoengineering for biological applications. Curr. Opin. Biotechnol 2022, 74, 247–255. [PubMed: 34998108]

(4). Griffin ME; Hsieh-Wilson LC Tools for mammalian glycoscience research. Cell 2022, 185, 2657–2677. [PubMed: 35809571]

(5). Zeng Y; Ramya TNC; Dirksen A; Dawson PE; Paulson JC High-efficiency labeling of sialylated glycoproteins on living cells. Nat. Methods 2009, 6, 207–209. [PubMed: 19234450]

(6). Li Q; Li Z; Duan X; Yi W A Tandem Enzymatic Approach for Detecting and Imaging Tumor-Associated Thomsen–Friedenreich Antigen Disaccharide. J. Am. Chem. Soc 2014, 136, 12536–12539. [PubMed: 25157422]

(7). Sun T; Yu S-H; Zhao P; Meng L; Moremen KW; Wells L; Steet R; Boons G-J One-Step Selective Exoenzymatic Labeling (SEEL) Strategy for the Biotinylation and Identification of Glycoproteins of Living Cells. J. Am. Chem. Soc 2016, 138, 11575–11582. [PubMed: 27541995]

(8). Wen L; Zheng Y; Jiang K; Zhang M; Kondengaden SM; Li S; Huang K; Li J; Song J; Wang PG Two-Step Chemoenzymatic Detection of N-Acetylneuraminic Acid–α(2-3)-Galactose Glycans. J. Am. Chem. Soc 2016, 138, 11473–11476. [PubMed: 27554522]

(9). Capicciotti CJ; Zong C; Sheikh MO; Sun T; Wells L; Boons G-J Cell-Surface Glyco-Engineering by Exogenous Enzymatic Transfer Using a Bifunctional CMP-Neu5Ac Derivative. J. Am. Chem. Soc 2017, 139, 13342–13348. [PubMed: 28858492]

(10). Jiang H; López-Aguilar A; Meng L; Gao Z; Liu Y; Tian X; Yu G; Ovryn B; Moremen KW; Wu P Modulating Cell-Surface Receptor Signaling and Ion Channel Functions by In Situ Glycan Editing. Angew. Chem. Int. Ed 2018, 57, 967–971.

(11). Gray MA; Stanczak MA; Mantuano NR; Xiao H; Pijnenborg JFA; Malaker SA; Miller CL; Weidenbacher PA; Tanzo JT; Ahn G; Woods EC; Läubli H; Bertozzi CR Targeted glycan degradation potentiates the anticancer immune response in vivo. Nat. Chem. Biol 2020, 16, 1376–1384. [PubMed: 32807964]

(12). Tang F; Zhou M; Qin K; Shi W; Yashinov A; Yang Y; Yang L; Guan D; Zhao L; Tang Y; Chang Y; Zhao L; Yang H; Zhou H; Huang R; Huang W Selective N-glycan editing on living cell surfaces to probe glycoconjugate function. Nat. Chem. Biol 2020, 16, 766–775. [PubMed: 32483376]

(13). Wulff G Molecular Imprinting in Cross-Linked Materials with the Aid of Molecular Templates—A Way towards Artificial Antibodies. Angew. Chem. Int. Ed. Engl 1995, 34, 1812–1832.

(14). Shinde S; El-Schich Z; Malakpour A; Wan W; Dizeyi N; Mohammadi R; Rurack K; Gjörloff Wingren A; Sellergren B Sialic Acid-Imprinted Fluorescent Core–Shell Particles for Selective Labeling of Cell Surface Glycans. J. Am. Chem. Soc 2015, 137, 13908–13912. [PubMed: 26414878]

(15). Stephenson-Brown A; Acton AL; Preece JA; Fossey JS; Mendes PM Selective glycoprotein detection through covalent templating and allosteric click-imprinting. Chem. Sci 2015, 6, 5114–5119. [PubMed: 29142730]

(16). Demir B; Lemberger MM; Panagiotopoulou M; Medina Rangel PX; Timur S; Hirsch T; Tse Sum Bui B; Wegener J; Haupt K Tracking Hyaluronan: Molecularly Imprinted Polymer Coated Carbon Dots for Cancer Cell Targeting and Imaging. ACS Appl. Mater. Interfaces 2018, 10, 3305–3313. [PubMed: 29299913]

(17). Medina Rangel PX; Laclef S; Xu J; Panagiotopoulou M; Kovensky J; Tse Sum Bui B; Haupt K Solid-phase synthesis of molecularly imprinted polymer nanolabels: Affinity tools for cellular bioimaging of glycans. Sci. Rep 2019, 9, 3923. [PubMed: 30850730]

(18). Wang SS; Ye J; Bie ZJ; Liu Z Affinity-tunable specific recognition of glycoproteins via boronate affinity-based controllable oriented surface imprinting. Chem. Sci 2014, 5, 1135–1140.

(19). Wang S; Yin D; Wang W; Shen X; Zhu J-J; Chen H-Y; Liu Z Targeting and Imaging of Cancer Cells via Monosaccharide-Imprinted Fluorescent Nanoparticles. Sci. Rep 2016, 6, 22757. [PubMed: 26948803]

(20). Dong Y; Li W; Gu Z; Xing R; Ma Y; Zhang Q; Liu Z Inhibition of HER2-Positive Breast Cancer Growth by Blocking the HER2 Signaling Pathway with HER2-Glycan-Imprinted Nanoparticles. Angew. Chem. Int. Ed 2019, 58, 10621–10625.

(21). Ortega-Caballero F; Rousseau C; Christensen B; Petersen TE; Bols M Remarkable supramolecular catalysis of glycoside hydrolysis by a cyclodextrin cyanohydrin. J. Am. Chem. Soc 2005, 127, 3238–3239. [PubMed: 15755115]

(22). Samanta M; Krishna VSR; Bandyopadhyay S A photoresponsive glycosidase mimic. Chem. Commun 2014, 50, 10577–10579.

(23). Sharma B; Striegler S Crosslinked Microgels as Platform for Hydrolytic Catalysts. Biomacromolecules 2018, 19, 1164–1174. [PubMed: 29547269]

(24). Striegler S; Sharma B; Orizu I Microgel-Catalyzed Hydrolysis of Nonactivated Disaccharides. Acs Catal 2020, 10, 14451–14456.

(25). Sharma B; Striegler S Nanogel Catalysts for the Hydrolysis of Underivatized Disaccharides Identified by a Fast Screening Assay. Acs Catal 2023, 13, 1614–1620.

(26). Li X; Zhao Y Synthetic glycosidases for the precise hydrolysis of oligosaccharides and polysaccharides. Chem. Sci 2021, 12, 374–383.

(27). Li X; Zangiabadi M; Zhao Y Molecularly Imprinted Synthetic Glucosidase for the Hydrolysis of Cellulose in Aqueous and Nonaqueous Solutions. J. Am. Chem. Soc 2021, 143, 5172–5181. [PubMed: 33759517]

(28). Zangiabadi M; Zhao Y Synergistic Hydrolysis of Cellulose by a Blend of Cellulase-Mimicking Polymeric Nanoparticle Catalysts. J. Am. Chem. Soc 2022, 144, 17110–17119. [PubMed: 36069714]

(29). Awino JK; Gunasekara RW; Zhao Y Selective Recognition of d-Aldohexoses in Water by Boronic Acid-Functionalized, Molecularly Imprinted Cross-Linked Micelles. J. Am. Chem. Soc 2016, 138, 9759–9762. [PubMed: 27442012]

(30). Gunasekara RW; Zhao Y A General Method for Selective Recognition of Monosaccharides and Oligosaccharides in Water. J. Am. Chem. Soc 2017, 139, 829–835. [PubMed: 27983819]

(31). Leyva E; Young MJT; Platz MS High yields of formal CH insertion products in the reactions of polyfluorinated aromatic nitrenes. J. Am. Chem. Soc 1986, 108, 8307–8309.

(32). Lairson LL; Withers SG Mechanistic analogies amongst carbohydrate modifying enzymes. Chem. Commun 2004, 2243–2248.

(33). Zechel DL; Withers SG Glycosidase mechanisms: Anatomy of a finely tuned catalyst. Acc. Chem. Res 2000, 33, 11–18. [PubMed: 10639071]

(34). Li S-F; Cheng F; Wang Y-J; Zheng Y-G Strategies for tailoring pH performances of glycoside hydrolases. Crit. Rev. Biotechnol 2021, 1–21.

(35). Becker D; Braet C; Brumer H 3rd; Claeyssens M; Divne C; Fagerström BR; Harris M; Jones TA; Kleywegt GJ; Koivula A; Mahdi S; Piens K; Sinnott ML; Ståhlberg J; Teeri TT; Underwood M; Wohlfahrt G Engineering of a glycosidase Family 7 cellobiohydrolase to more alkaline pH optimum: the pH behaviour of Trichoderma reesei Cel7A and its E223S/ A224H/L225V/T226A/ D262G mutant. Biochem. J 2001, 356, 19–30. [PubMed: 11336632]

(36). Harvey DJ; Wing DR; Kuster B; Wilson IB Composition of N-linked carbohydrates from ovalbumin and co-purified glycoproteins. J. Am. Soc. Mass Spectrom 2000, 11, 564–571. [PubMed: 10833030]

(37). Song XZ; Ju H; Lasanajak Y; Kudelka MR; Smith DF; Cummings RD Oxidative release of natural glycans for functional glycomics. Nat. Methods 2016, 13, 528–534. [PubMed: 27135973]

(38). Prien JM; Ashline DJ; Lapadula AJ; Zhang H; Reinhold VN The high mannose glycans from bovine ribonuclease B isomer characterization by ion trap MS. J. Am. Soc. Mass Spectrom 2009, 20, 539–556. [PubMed: 19181540]

(39). Choi O; Tomiya N; Kim JH; Slavicek JM; Betenbaugh MJ; Lee YC N-glycan structures of human transferrin produced by Lymantria dispar (gypsy moth) cells using the LdMNPV expression system. Glycobiology 2003, 13, 539–548. [PubMed: 12672704]

(40). Lu G; Holland LA Profiling the N-Glycan Composition of IgG with Lectins and Capillary Nanogel Electrophoresis. Anal. Chem 2019, 91, 1375–1383. [PubMed: 30525457]

(41). Yang BY; Gray JS; Montgomery R The glycans of horseradish peroxidase. Carbohydr. Res 1996, 287, 203–212. [PubMed: 8766207]

(42). Schauer R Sialic acids as regulators of molecular and cellular interactions. Curr. Opin. Struct. Biol 2009, 19, 507–514. [PubMed: 19699080]

(43). McArthur JB; Yu H; Tasnima N; Lee CM; Fisher AJ; Chen X α2–6-Neosialidase: A Sialyltransferase Mutant as a Sialyl Linkage-Specific Sialidase. ACS Chem. Biol 2018, 13, 1228–1234. [PubMed: 29543427]

(44). Chen X; Varki A Advances in the Biology and Chemistry of Sialic Acids. ACS Chem. Biol 2010, 5, 163–176. [PubMed: 20020717]

(45). Viswanathan K; Chandrasekaran A; Srinivasan A; Raman R; Sasisekharan V; Sasisekharan R Glycans as receptors for influenza pathogenesis. Glycoconj. J 2010, 27, 561–570. [PubMed: 20734133]

(46). Ren L; Qin X; Cao X; Wang L; Bai F; Bai G; Shen Y Structural insight into substrate specificity of human intestinal maltase-glucoamylase. Protein Cell 2011, 2, 827–836. [PubMed: 22058037]
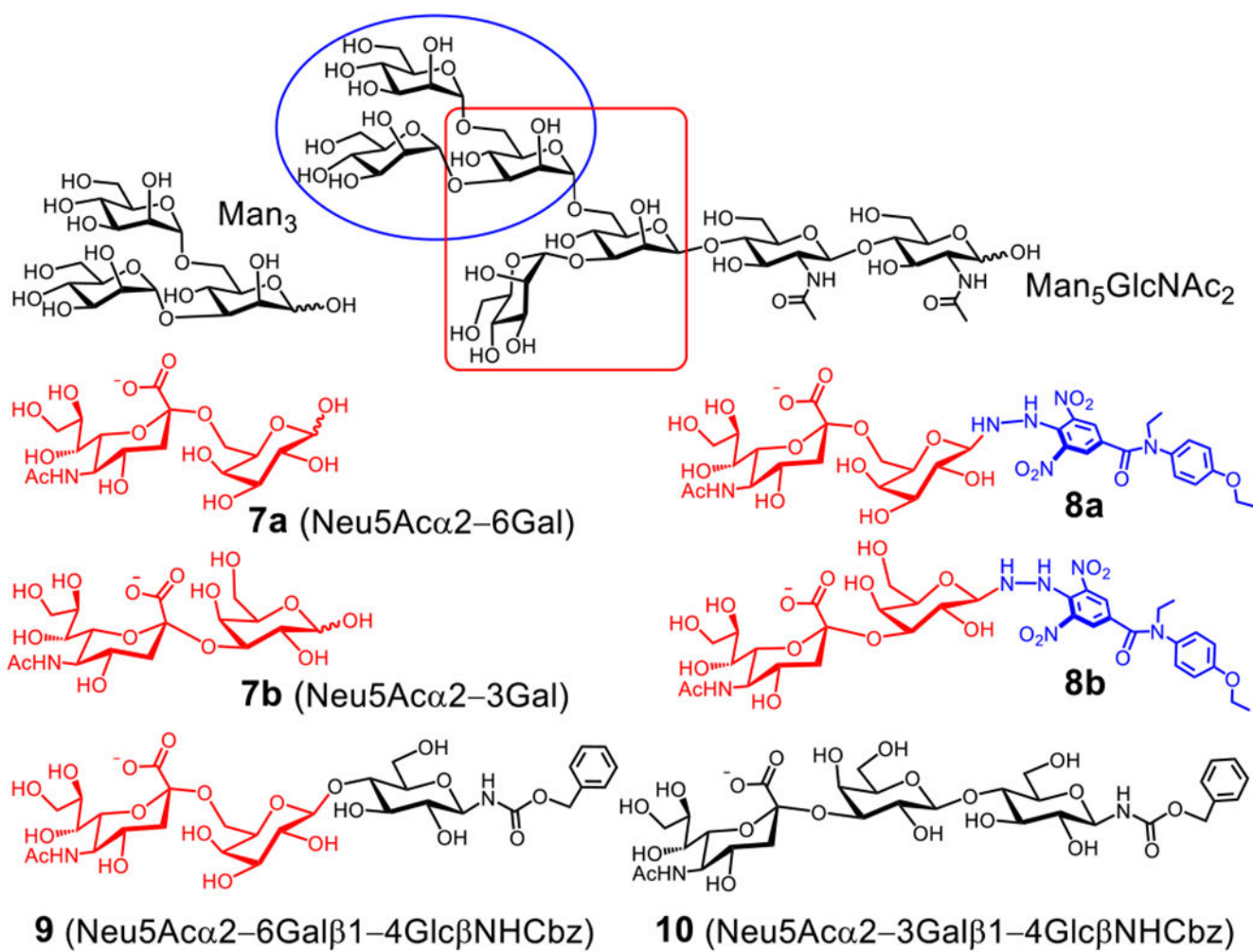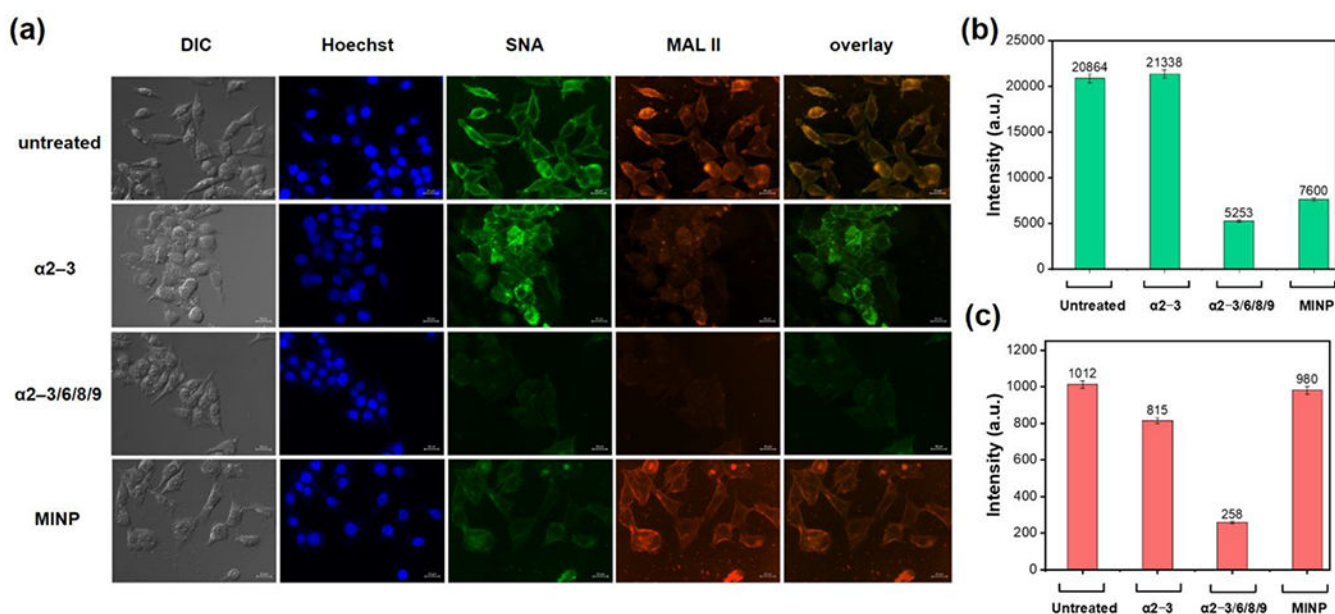
Figure 1.
Structures of key glycans used in this work.
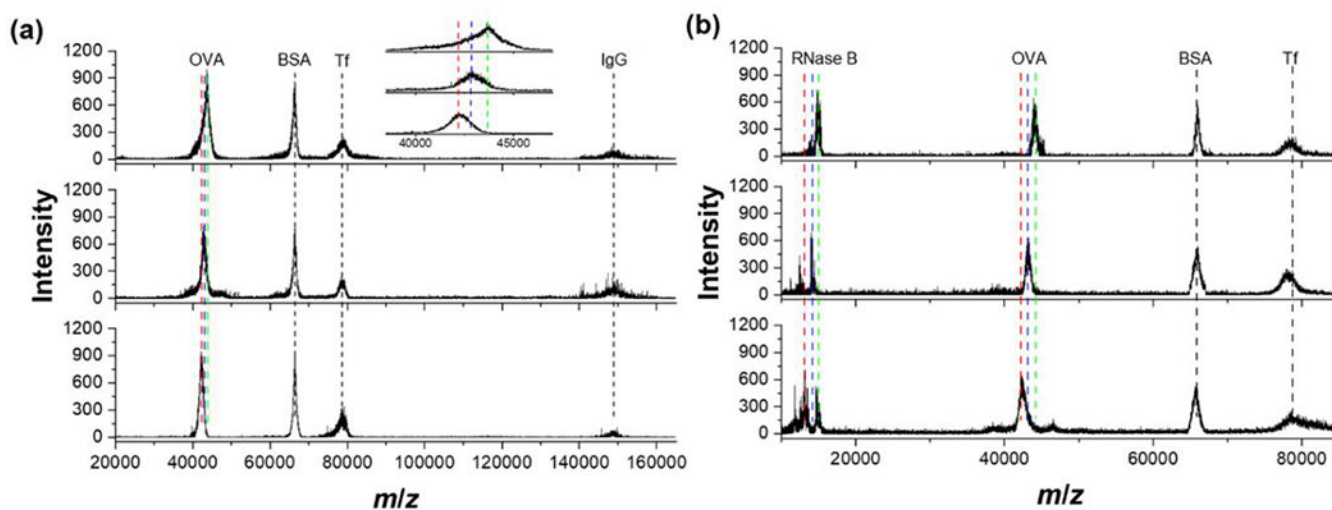
Figure 2.
MALDI spectra of (a) OVA/BSA/Tf/IgG and (b) RNase B/OVA/BSA/Tf. The spectra are for the untreated protein mixture, protein mixture treated with $MINP_{Man3}$-COOH, and protein mixture treated with $MINP_{OVA}$-COOH from top to bottom. The inset in Figure 2a shows the expanded OVA peak with the desired cleavages. The cleavage was performed with [protein] = 5 mg/mL and [MINP] = 0.5 mg/mL at 37°C for 24 h.

Figure 3.
(a) Fluorescence imaging of MDA-MB-231 cells under bright field image, in the blue
channel (to visualize the nucleus-binding Hoechst 33342), in the green channel (to visualize
Neu5Acα2–6Gal stained by FITC-SNA I), in the red channel (to visualize Neu5Acα2–3Gal
stained by biotinylated MAL-II lectin and Rhodamine-labelled streptavidin), and overlay of
the green and red channel. The cells were untreated and treated with an α2–3-sialidase, a
nonspecific α2–3/6/8/9 sialidase, and MINP$_{7a}$-COOH (functionalized with surface ligand
6b so that the MINPs were not internalized by cells), respectively, from top to bottom.
(b) Fluorescent intensity of differently treated MDA-MB-231 cells in the green channel
determined by FACS. (b) Fluorescent intensity of differently treated MDA-MB-231 cells in
the red channel determined by FACS.
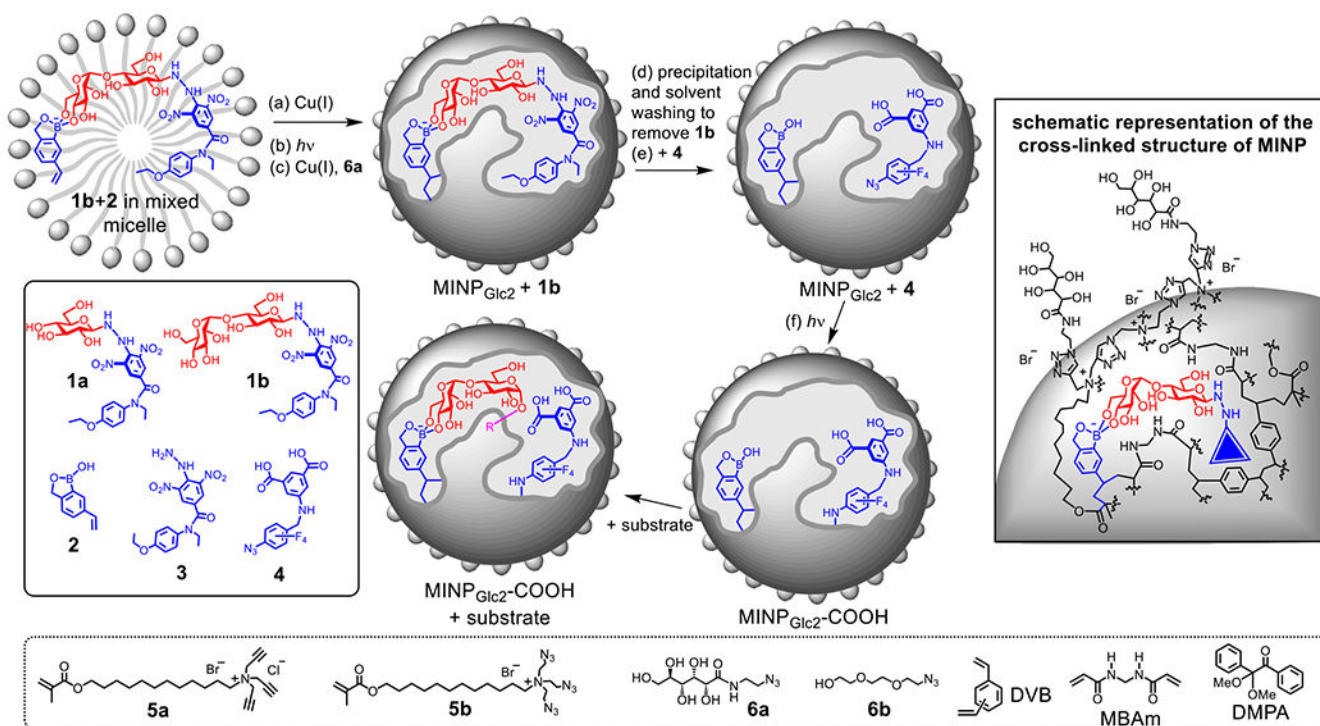
Scheme 1.
Preparation of a glycan-cleaving catalyst from molecular imprinting of a cross-linked micelle, with the surface ligands omitted for clarify. A schematic representation of MINP$_{Glc2}$ with the boroxole-bound template **1b** is shown in the right panel.

Table 1.

Binding properties of MINPs determined by isothermal titration calorimetry (ITC).[a]

entry	host	guest[b]	K_a ($\times 10^3$ M^{-1})	K_{rel}[c]
1	MINP$_{Glc1}$	**4**	425 ± 23	-
2	MINP$_{Glc1}$	Glc$_1$	4.24 ± 0.26	1
3	MINP$_{Glc1}$	Glc$_2$	1.22 ± 0.31	0.29
4	MINP$_{Glc1}$-COOH	Glc$_1$	9.51 ± 0.87	1
5	MINP$_{Glc1}$-COOH	GlC$_2$	2.41 ± 0.62	0.25
6	MINP$_{Glc1}$-COOH	Glc$_4$	2.21 ± 0.33	0.23
7	MINP$_{Glc2}$	Glc$_1$	1.48 ± 0.62	0.13
8	MINP$_{Glc2}$	Glc$_2$	11.3 ± 1.14	1
9	MINP$_{Glc2}$-COOH	Glc$_1$	4.26 ± 0.73	0.10
10	MINP$_{Glc2}$-COOH	Glc$_2$	42.3 ± 1.58	1
11	MINP$_{Glc2}$-COOH	Glc$_4$	10.4 ± 1.24	0.25
12	MINP$_{Man3}$-COOH	Man$_3$	3.79 ± 0.22	1
13	MINP$_{Man3}$-COOH	OVA	2.51 ± 0.23	0.66
14	MINP$_{OVA}$-COOH	OVA	1.78 ± 0.36	1
15	NINP	Glc$_1$	<0.01	

[a] Titrations were performed in duplicates with the indicated errors in 10 mM MES buffer (pH 6.5) at 298 K.

[b] Glc$_1$, Glc$_2$, and Glc$_3$ refer to glucose, maltose, and maltotriose, respectively.

[c] K_{rel} is the binding constant of a guest relative to that of the templating sugar for a particular MINP.